Low Order Wavefront Sensing and Control for Exoplanet Imaging

Milestone White Paper

NASA Strategic Astrophysics Technology Program

Principal Investigator: *John Trauger*

Co-Investigators:

J. Kent Wallace, John Krist, A.J. Riggs, Duncan Liu (JPL)

Collaborators:

David Salvage (AOX), Byoung-Joon Seo (JPL)

15 May 2024

Jet Propulsion Laboratory
California Institute of Technology

Signature Page

E-SIGNED by John Trauger
on 2024-05-15 18:15:47 GMT

John Trauger Date

Principal Investigator

E-SIGNED by Brendan Crill
on 2024-05-15 18:16:28 GMT

Brendan Crill Date

Deputy Program Chief Technologist, ExEP

E-SIGNED by Nicholas Siegler
on 2024-05-15 22:41:44 GMT

Nick Siegler Date

Program Chief Technologist, ExEP

E-SIGNED by Lucas Paganini
on 2024-05-15 19:06:19 GMT

Lucas Paganini Date

ExEP Program Executive, NASA HQ

Low Order Wavefront Sensing and Control for Exoplanet Imaging

SAT Milestone White Paper

Table of Contents

1) Objectives

The Astro2020 decadal report [1] calls for the maturation of enabling technologies for the next flagship-class space observatory, now envisioned as the Habitable Worlds Observatory (HWO). A central objective of this mission is the direct imaging and spectroscopy of exoplanet systems in reflected starlight. Concepts for an actively corrected coronagraph instrument for extreme high contrast imaging have been extensively explored and tested in laboratory investigations over the past decade. Many of the current coronagraph technologies will be validated in flight with the Coronagraph Instrument (CGI) on the Nancy Grace Roman Telescope [2]. Nevertheless, currently-demonstrated technologies fall short, by an order of magnitude or more, of the sensitivities needed to detect earth-sized exoplanets orbiting at earth-like distances from the star in reflected starlight, as articulated in the NASA Exoplanet Exploration Program's (ExEP) list of Coronagraph/Telescope Technology Gaps [3] that calls for direct imaging at exoplanet/star raw contrast ratios of 10^{-10} or better in visible wavelengths, with 10% throughput or better, and for exoplanet-star separations of 3 λ/D or smaller in a dynamic space-simulating environment [4].

Development of new hardware solutions to known technology challenges must be initiated in this decade, in concert with the NASA HWO programs for technology maturation. The critical enabling technologies must be developed, refined, understood, and matured to the level where they can be incorporated into nascent mission concepts with solid confidence that they will reduce engineering risk and mission cost. This proposal addresses the challenge of low-order wavefront stabilization in a high-contrast coronagraph on a dynamic space-based observatory.

Our objective is the demonstration of complex (amplitude and phase) optical wavefront control at a level required for $1x10^{-10}$ contrast across a 10% spectral bandwidth in a *dynamic* coronagraph testbed environment. Wavefront control at this level is a fundamental physics requirement for the creation and maintenance of the high-contrast dark field for any optical coronagraph. It is a challenge that must be met regardless of the coronagraph architecture chosen for the HWO coronagraph, whether it be hybrid Lyot, vortex, or another configuration. The most straightforward way to validate the required *wavefront control technology* is by demonstration in the context of a laboratory coronagraph system operating at contrasts at or near $1x10^{-10}$. Demonstrations at this level are necessary to assure that significant sources of error have been unambiguously identified and effectively controlled or mitigated.

We recognize that wavefront errors will occur over two distinctly different frequency regimes. Observatory pointing jitter, alignment drifts, and thermal distortions across large structures, originating from outside influences, for even the most stable observatory structures, will require active maintenance through a closed-loop low-order wavefront sensing-and-control system operating on time scales from milliseconds to minutes. On the other hand, extreme high contrast imaging requires high-order wavefront control using one or a pair of deformable mirrors to control both amplitude and phase of the wavefront, which is achieved via the Talbot effect [5] through time-intensive iterative on-sky techniques [6,7,8]. The corresponding high-order DM surface figure settings must be maintained open-loop over times comparable to on-target science integration times, while relying on thermal and mechanical isolation of the coronagraph instrument from exterior influences.

Our objective is the implementation and closed-loop demonstration of a new low-order wavefront control (LOWFC) element – a hardware component for the active correction of wavefront errors associated with telescope line-of-sight jitter, thermal gradients, and alignment

drift. This hardware, when incorporated into a laboratory coronagraph and used in concert with a next-generation Hybrid Lyot Coronagraph (HLC) focal plane mask and Zernike wavefront sensor (ZWFS), will test the concept at high levels of contrast in a dynamic testbed environment, thereby providing confidence that significant sources of error have been unambiguously identified and effectively controlled or mitigated. The proposed investigation addresses a gap among the technologies required for exoplanet imaging as defined by the Astro2020 report.

2) Overview / Background

We combine optical modeling, improvements in the design and fabrication of the laboratory coronagraph elements, characterization of existing deformable mirrors to high levels of precision, and the addition of a new active optical element for the low order corrections. We utilize the facilities that have been assembled in our Exoplanet Imaging Technology Laboratory, where testing and calibrations of coronagraph components and systems can be carried out to the required precision in a vacuum environment. This laboratory is ideally suited for the coordination of component fabrication and testing, incremental improvements in testbed optical performance, and refinements in operational techniques. This work also serves as preparation and justification for further work at the highest level in the Decadal Survey Testbed (DST).

Separation of active low-order and stable high-order elements of wavefront control. We will implement and demonstrate a new hardware control element to actively stabilize the pointing jitter and low-order Zernike wavefront terms within a single integrated tip/tilt/surface-parallel deformable mirror (SPA/DM) assembly guided by feedback from a low order wavefront sensor (LOWFS).

Our approach is a departure from current exoplanet instrument concepts. LUVOIR/ECLIPS and Habex/HCG each utilize a pair of high order deformable mirrors (DMs) to create a high contrast dark field using the iterative EFC sensing and control process, which is reliant on thermal and mechanical isolation to maintain picometer-level instrument stability. The coronagraph instrument must be isolated from external disruptions including pointing jitter, alignment drift, and thermal distortions of large telescope elements, again to picometer levels. Both ECLIPS and HCG use a fast-steering mirror (FSM) to correct pointing jitter. Focus drift may be compensated by motions of the telescope secondary mirror, but this method is not well suited to active correction. Therefore, the stabilization of focus, astigmatism, coma, and other low order wavefront terms required the active superposition of corrective shapes onto the high order DMs. This is disruptive to the otherwise stable surface patterns on the high order DMs, may exceed the corrective range of the high-order DMs, and has never been demonstrated at the 10^{-10} contrast level.

The Roman/CGI has implemented wavefront control in the same manner as ECLIPS and HCG, but with the addition of a focus control mechanism (FCM) to offload telescope focus drift. The CGI project has performed the best demonstration to date of active low order control in a high contrast coronagraph. Contrast was corrected at the 10^{-8} level by the FSM and FCM in the presence of significant jitter and focus errors, but the high order DMs did not participate, and the correction of Zernike errors beyond focus was not demonstrated [9].

We will explore, through modeling and experiment, the effectiveness of separating wavefront control functions into an (a) active closed-loop control of low spatial frequencies followed by the (b) extremely stable open-loop control of the high spatial frequencies. It is essential that the low

order wavefront be actively maintained without the contamination of high order residual errors, else the effectiveness of high order control will be compromised.

We will procure, characterize, and test a LOWFC element with an inherently smooth optical surface that has minimal power to create or disrupt high-order wavefront solutions established by the DMs. All low-order corrections will be performed with a single LOWFC element. This element reduces the number of optical elements and hence the accumulation of optical wavefront errors in the highly corrected beam upstream of the coronagraph elements. Furthermore, fewer optical surfaces at planes intermediate between pupils reduce the effects of beam walk due to pointing errors, hence improving sensitivity to pointing jitter. This element also shields the high-order DMs from potentially large low-order errors that may exceed the control range of the DMs.

3) Milestone Definitions

Our performance goal is the demonstration of wavefront control and high-contrast coronagraph performance in the presence of low order disturbances of 1 nm rms or more, with sufficient fidelity to maintain coronagraph contrast of $5x10^{-10}$ or better over a dark field extending from 3 to 10 λ/D, in a 10% spectral band centered at 550 nm.

Work begins with detailed design of the optical layout for the experiment. All components will reside on a single optical table, all are configured for operation in the vibration-isolated 4x6 foot vacuum chamber located in the Exoplanet Imaging Technology Laboratory. The essential coronagraph and high-order DM components are already resident in the laboratory. The major new item will be the Surface Parallel Array / Deformable Mirror (SPA/DM), to be specified and purchased from AOX. The sequence of work is as follows. Some tasks can be performed in parallel. A schedule chart with the key milestones follows in Section 7.

Phase 1a Milestone. Upgrade the Compact Coronagraph Testbed (CCT) and verify end-to-end functionality.

- Update the optical design of the CCT coronagraph to accommodate the LOWFC element.
- Work with AOX to finalize the design for the SPA/DM and its tip/tilt element, comprising the LOWFC. Design trades and specifications will be modeled and evaluated. Place the purchase order with AOX.
- Specify and acquire the optical mounts etc. as required for the updated testbed layout.
- Assemble and align the coronagraph elements on the CCT optical table in air under the laboratory clean tent, with a surrogate flat mirror standing in for the SPA/DM.
- In air, operate the coronagraph to verify alignments, ensure functionality, and inspect for sources of stray light. Verify operation of all optical and electronic elements end-to-end, from the supercontinuum source through to the CCD cameras.

Phase 1b Milestone. Verify CCT baseline performance; test and calibrate the SPA/DM.

- Transfer the CCT into the 4x6 foot vacuum chamber. Verify readiness of the FALCO software implementation for EFC probing and high-order DM control. Establish baseline contrast performance of $5x10^{-10}$ or better with the surrogate flat in place of the SPA/DM. To the extent possible, identify and mitigate any sources of noise, stray light, or other factors that may prevent the achievement of contrast performance predicted by models (see *Appendix*). Upon completion, return the CCT to the laboratory clean tent.

- Receive the LOWFC assembly from AOX. Mount the device in the Twyman-Green vacuum interferometer (VSG) for component level measurements of its optical and wavefront control characteristics in the vacuum. Measure the SPA/DM surface figure and response to commands for low order Zernike shapes. Investigate creep, drift, hysteresis following actuation. Fold these results into the optical model, quantify the achievable levels of control for low order Zernike terms Z4-Z8 (focus, astigmatism, and coma).

Phase 2a Milestone. Demonstrate closed-loop wavefront control with SPA/DM.

- Mount the LOWFC device on the coronagraph table, in air under the clean tent. Align the optics. Verify operation of the ZWFS for tip/tilt offsets.
- Verify readiness of software for Zernike low-order wavefront analysis and SPA/DM control of tip/tilt and low order corrections.
- Introduce low order wavefront errors, evaluate the ability of the ZWFS system to accurately sense and translate the ZWFS signal into corrective signals for the SPA/DM.

Phase 2b Milestone. Low-order wavefront stabilization concurrent with high-contrast imaging.

- Transfer the CCT coronagraph table system once again to the 4x6 foot vacuum chamber. Re-establish and monitor the baseline high contrast dark field and evaluate its stability and any anomalies.
- Introduce low order wavefront errors, use the ZWFS&LOWFC control loop to null out the low order error, evaluate maintenance and stability of the high contrast dark field. All laboratory tests will be performed three times each to show repeatability.
- Perform predictive and post-test diffractive modeling to fully understand the laboratory results and limitations. Mitigate limiting factors to the extent possible.
- Report significant results in the open literature, followed by the final report.
- Evaluate the potential merits of transferring the LOWFC technology to one of the Decadal Survey Testbed setups as a facility enhancement for future demonstrations at potentially higher levels of performance.
- When successful, this technology demonstration of the SPA/DM assembly/component in a relevant environment (ZWFS control loop, high-contrast coronagraph, vacuum testbed) at relevant levels of contrast performance would qualify as a TRL 5 technology development.

4) Description of the Experiment

Laboratory coronagraph testbed. This proposal addresses a universal requirement for coronagraph wavefront control. We have a choice of coronagraph architectures for the proposed demonstrations, many of which would be appropriate for the task. The hybrid Lyot coronagraph (HLC) is baselined for these demonstrations. Versions of the HLC have consistently demonstrated 4-6 $x10^{-10}$ normalized intensity (dark field contrast) over a 10% spectral bandwidth in the laboratory [3, 10, 11]. The laboratory DST employed a simple Lyot coronagraph for its initial commissioning demonstrations, yielding a contrast of $4x10^{-10}$ over a 10% spectral bandwidth [11]. A handful of experimental factors, each contributing contrast degradations of order 10^{-10} in the commissioning demonstrations, have been identified by the DST commissioning team and will be addressed in this work. The HLC is the primary coronagraph

mode for imaging demonstrations in the Roman CGI [2] and was identified as among the leading coronagraph options for HabEx and LUVOIR [12,13].

The HLC is among the simplest architectures for high contrast coronagraphy. As such, the fabrication and testing of its most critical element, the focal plane mask (FPM), is relatively straightforward using conventional fabrication and optical measuring techniques. Simplicity of the HLC architecture, with just one transmissive element (the FPM is formed on a fused silica substrate) and a minimum of other complications (no additional transmissive or polarizing elements in the highly corrected wavefront upstream of the Lyot stop), minimizes uncertainties in performance modeling, estimation of manufacturing tolerances, and sensitivity to experimental imperfections, supporting a reliable comparison between predicted and demonstrated performance. The intention is to use a simple, high-performing, and well-understood coronagraph to test and evaluate the LOWFC element in its operational environment. The tolerances to real-world optical imperfections in the coronagraph instrument, and in particular the requirements placed on the corrective LOWFC element, will be the subject of study in this work.

The optical layout of the Compact Coronagraph Testbed (CCT) is sketched in Figure 1. One new element, the Low Order Wavefront Corrector (LOWFC), is added to the previous layout. Light proceeds from a source at left to the coronagraph image at right. The focusing elements are off-axis paraboloidal (OAP) mirrors, depicted in this unfolded layout as "lenses." As indicated, the optical system leapfrogs between pupil planes and focal planes. Located in the pupil planes are the LOWFC, the high-order DM1, and the Lyot stop. The source pinhole, coronagraph FPM and CCD imager are located at focal planes. The Zernike Wavefront Sensor (ZWFS) signal is taken in reflection from the FPM. For laboratory experiments the "telescope" is replaced by a surrogate "star," and an iris at the location of the LOWFC becomes the defining pupil for the system. Not included in the sketch is a field stop intermediate between the final OAP and CCD imager.

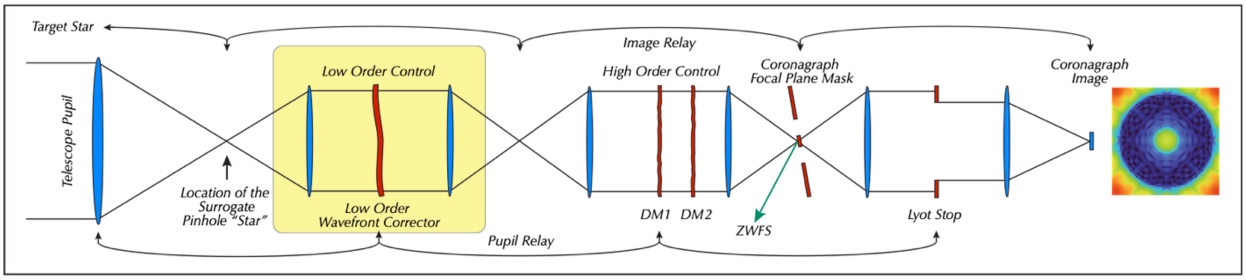

Figure 1. *Sketch of the optical layout of the CCT coronagraph. The new element, the Low Order Wavefront Corrector (LOWFC), is highlighted.*

Deformable mirror for active low-order wavefront control. As indicated in the highlighted area of Figure 1, we introduce a new optical element into the CCT for the correction of low order wavefront errors. We will investigate the performance of a surface parallel deformable mirror technology developed by AOX that achieves low order corrective figure by applying stress to the backside of a flat optical substrate [14]. As indicated in Figure 2, a patterned sheet is formed as a stack of lead-magnesium-niobate (PMN) ceramic layers interleaved with embedded conductive layers, essentially a capacitor structure, comprising an array of hexagonal "surface parallel" active elements bonded to the backside of the substrate. Voltage applied to individual actuators

cause a surface-parallel tensile stress. The mirror substrate bends in response to the collective stress across the actuator array.

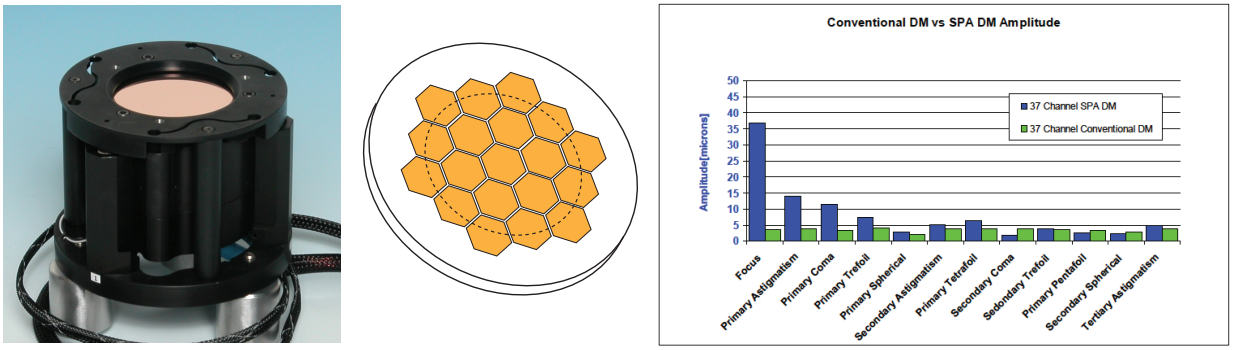

Figure 2. *Low order wavefront corrector (LOWFC) comprising a surface-parallel actuated deformable mirror (SPA/DM) mounted in a tip/tilt flexure stage. At left, the tip/tilt flexure stage. At center, sketch of a multilayer web of hexagonal PMN electrostrictive ceramic is bonded to the backside of the thin polished mirror substrate. The dashed circle indicates the active pupil -- the area outside the circle will be masked off. Control authority is greatest for the lowest order Zernike terms and strongly diminished for the higher Zernike terms, as seen in the representative response diagram at right.*

DM design parameters include the thickness of the substrate and shape and number of surface-parallel actuators. Increasing the thickness of the substrate suppresses the amplitude and range of spatial frequencies that can be formed by the DM. Our design objective is a polished DM surface capable of only low order Zernike shapes, with amplitude capabilities adequate for correction of the anticipated system errors. As shown in Figure 2, that control authority is greatest for the lowest Zernike orders and strongly diminished for the higher order terms, providing the greatest control authority for the focus, astigmatism, and lowest order terms that are expected to dominate the observatory wavefront errors. The surface parallel DM (SPA/DM) is mounted in a tip/tilt flexure assembly, as illustrated in Figure 2. The assembly now becomes the low order wavefront corrector (LOWFC), a single element in the optical system that corrects jitter and the expected levels of low order distortions and drift we expect for a large space observatory.

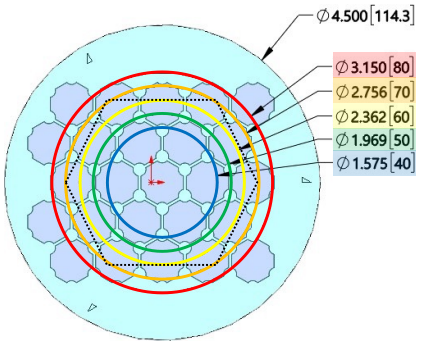

3 Point Mount on Ø60mm Aperture

	P-V [µm]	rms [µm]	Residual P-V [µm]	Residual rms [µm]	Correctability [%]	Stroke [ppm]
Power (Defocus)	3.71	1.07	0.067	0.014	98.72	50
Pri Astigmatism	0.54	0.11	0.049	0.004	96.85	50
Pri Coma	1.10	0.20	0.111	0.017	91.20	50
Pri Trefoil	0.97	0.17	0.185	0.015	91.52	50
Pri Spherical	0.64	0.18	0.174	0.037	79.01	50
Sec Astigmatism	0.16	0.04	0.083	0.008	80.39	50
Pri Tetrafoil	0.28	0.04	0.039	0.003	93.29	50
Sec Coma	0.93	0.19	0.415	0.060	68.82	50
Sec Trefoil	1.61	0.41	0.870	0.102	75.26	50

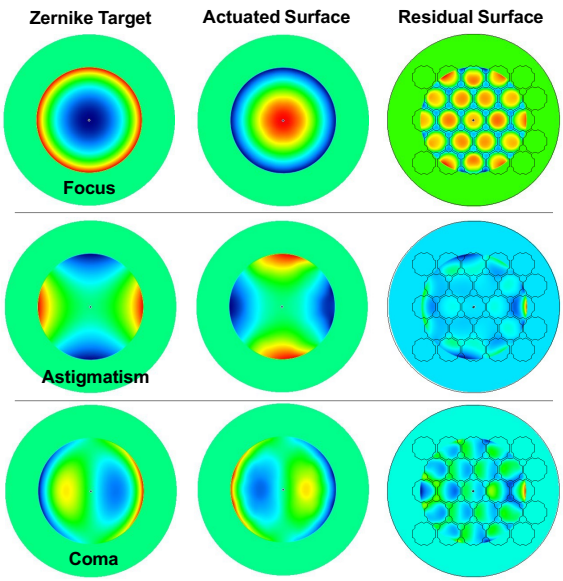

Figure 3. *Analysis of the preliminary SPA/DM design provided by AOX. This design adapts a commercial product line at AOX to the requirements of this experiment. At upper left, we select a working pupil diameter of 60 mm (yellow circle), an active area that is controlled by the central nineteen hexagonal PMN elements. Table at lower left indicates correctability of the focus, astigmatism, and coma terms of 98.7%, 96.9%, and 91.2% respectively. The nature of the relatively minor residual surface errors is illustrated by the images at right. Further design refinements will be considered once we initiate contract negotiations with AOX.*

Our experiments will test the ability of the LOWFC element to create and correct low order Zernike surface shapes while introducing a minimum of spurious high-order errors. We illustrate the importance of low-order wavefront control for the representative case of the hybrid Lyot coronagraph (as described below and illustrated in Figure 4). For this coronagraph, operating at ~10^{-10} contrast over a 10% bandwidth at 550 nm wavelength, the background speckle intensity averaged over the dark field will increase quadratically with the low-order Zernike term. For example, a Z4 focus term contributes $\Delta C = a$ x $(z4rms)^2$, with coefficient $a \sim 4.6\text{x}10^{-8}$ nm^{-2}. Hence 0.125 nm rms of Z4 focus adds $8\text{x}10^{-10}$ to the dark field contrast floor, 0.25 nm rms of Z4 adds $3\text{x}10^{-9}$, etc. The coefficients for focus, astigmatism, coma, trefoil, and spherical are $a \sim 4.6$, 6.4, 31.4, 4.1, and 138 x10^{-8} nm^{-2} respectively. Given that our milestone objectives are to be performed at $5\text{x}10^{-10}$ contrast or better, the LOWFS&C element is called on to stabilize the low-order terms to 0.1 nm rms or (much) better. The Zernike sensor has been demonstrated to measure phase with sub-picometer precision [16,17].

The SPA/DM and the LOWFS&C control loop will be tested and calibrated in our Vacuum Surface Gauge (VSG), a Twyman-Green phase-shifting interferometer operating in a 4x6 foot vacuum chamber. The VSG measures phase patterns across the aperture of the DM with noise levels of 20 picometers rms or better in single measurements, as has been demonstrated over the past decade and most recently in characterizations of 48x48 AOX DMs for the Roman/CGI project. Trends in high-order DM drift can be tracked to picometer rms / hour levels in the VSG.

Closed-loop experiments will introduce low-order errors, on the order of 1 nm rms or more, into the input beam of the CCT coronagraph, where the ZWFS [15,16,17] and LOWFC will be responsible for detecting and correcting the error. Simple tests of the control loop will apply low order distortions to the SPA/DM that are unknown to the ZWFS, then call on the LOWFS&C control system to make the corrections. A more definitive test is to use the high-order DM to introduce clean low order Zernike errors unknown to the ZWFS, to be sensed and corrected independently by the LOWFS&C system. This second experiment exploits the independence of the legacy pairwise-probing/EFC and the new ZWFS&C wavefront sensing and control methods. Other schemes for experimentally introducing low order errors will be considered. For example, low order errors could be introduced by stressing an optical flat upstream at yet another pupil in the system. We plan to do the first two experiments and not the third, as this would require additional optics, mounts, and unnecessary complications.

This test mimics the dominant wavefront errors in a large space observatory, where line-of-sight jitter, thermal gradients across the primary and secondary mirrors and structures, and misalignments of the telescope primary and secondary mirrors introduce their dominant errors at the entrance pupil of the system.

This test is most relevant for observatory architectures that minimize the number of intermediate fold and focusing elements between the telescope and the coronagraph. This approach is exemplified in the Exo-C concept study [18] and the earlier ACCESS concept study [19] which anticipated the wavefront control issues addressed in this proposal. Exo-C minimizes the number of error-introducing optical elements upstream of the coronagraph and, further, by combining a jitter-correcting tip/tilt stage with the first of its two high-order DMs.

The proposed experiments will determine the ability of this assembly to make well-formed corrections to low-order Zernike distortions without introducing spurious high-order artifacts. Demonstrated performance will be compared with engineering models of the LOWFC structure. Testbed performance will be optimized to the extent possible in the laboratory setting.

The Hybrid Lyot Coronagraph. The hybrid Lyot focal plane mask has been developed in a previous SAT2016 task [20]. This FPM design performance is consistent with requirements featured in the ExEP technology gap list: $1x10^{-10}$ contrast in a dark field with an inner working angle (IWA) of 3 λ/D at visible wavelengths, over a 10% spectral bandwidth, with throughput greater than 10% [3].

The FPM is comprised of thin terraced layers of nickel and a uniform layer of MgF_2 on a fused silica glass substrate, as illustrated in Figures 5 and 6. Diameter of the nickel element is 101.6 μm, appropriate for a 550 nm center wavelength, 10% spectral bandwidth, and a 3 λ_0/D inner working angle in an f/33 beam. Quality of the FPM substrate requires special consideration as the single transmitting element in the highly-corrected optical wavefront. The substrate material is Corning class-0A homogeneous fused silica, slightly wedged and AR coated on the backside to suppress and remove reflective ghosts from the beam.

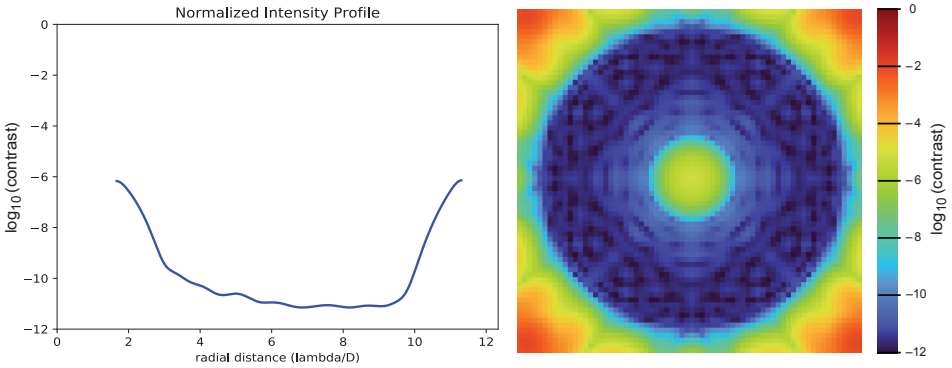

Figure 4. *Normalized intensity computed for the FPM shown in Figures 5 and 6. At left is the azimuthally averaged dark-field intensity. Contrast is $1x10^{-10}$ or better across the dark field in 10% bandwidth light centered at 550 nm wavelength (contrast is $1.4x10^{-11}$ when averaged over the entire dark field). At right, an illustration of the 360° dark field extending from 3 to 10 λ_0/D.*

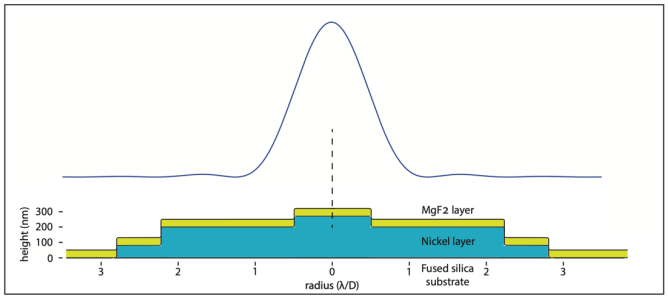

Figure 5. *Cross section of the circular metal-dielectric focal plane mask design consisting of a terraced-thickness nickel layer and a uniform-thickness overlayer of magnesium fluoride. The central Zernike phase dimple enables low-order wavefront error sensing. Also shown for scale is the cross section of the Airy point spread function (PSF) at 550 nm wavelength.*

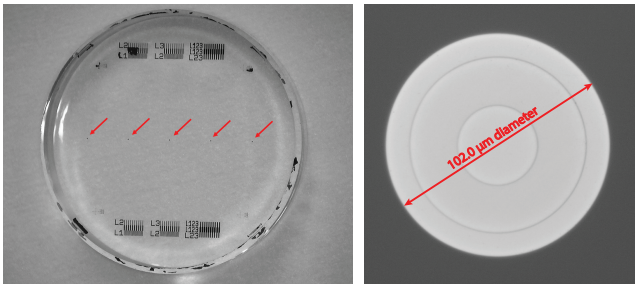

Figure 6. *Terraced-thickness HLC masks manufactured by SILIOS (France). Five identical copies, spaced by 4 mm, have been formed on the first surface of a grade 0A fused silica substrate. The full diameter of the FPM is 102 microns, corresponding to a radius of 2.8 λ/D in an f/33 beam at 550 nm wavelength. Substrate has a diameter of 25.4 mm, thickness of 6.4 mm, and is AR coated on the backside.*

One or more DMs are used to control both phase and (phase-induced) amplitude across the coronagraph wavefront which, due to the Talbot effect, are each comparably significant at 10^{-10}

levels of contrast. High order wavefront control has been extensively demonstrated in the JPL high-contrast coronagraph testbeds, has been implemented in the Roman/CGI coronagraph, and was baselined for LUVOIR/ECLIPS and Habex/HCG instrument concepts.

For example, contrast performance was computed for the coronagraph sketched in Figure 1 with the focal plane mask in Figures 5 and 6 and a pair of 48x48 actuator deformable mirrors from AOX, a technology that has matured to TRL6 and will fly with the Roman CGI. The DM surface patterns are derived using the FALCO software package [21,22,23,24]. Starting with flat DMs in a perfect optical system, the solutions are derived via several tens of iterative computations. The result, shown in Figure 4, is a 360° high contrast dark field extending from 3 to 10 λ/D in 10% bandwidth "starlight" centered at 550 nm wavelength, with contrast better than 10^{-10} and throughput greater than 12%.

We note that solutions for a 180° half dark field are also possible using just one DM, as has been demonstrated in earlier work [10]. For our main objective, the precise stabilization of low order errors as required for the maintenance of the high order wavefront solution, the demonstrations can be carried out with either a 180° or 360° high contrast dark field of view. For simplicity and emphasis on the main objective of this proposal, we will perform the experiments with a single DM, retaining the option of reconfiguring for a pair of DMs if time and resources allow.

The FPM plays a central role in the Zernike wavefront sensing of low order wavefront errors. A central Zernike phase dimple on the FPM, as shown in Figure 5, modulates the starlight reflected by the FPM. The reflected light is reimaged in a LOWFS camera, where the low order errors can be extracted by analysis. The Zernike phase-contrast technique offers advantages for wavefront sensing. The device is intrinsically simple. It is a small (~1 λ/D in diameter) phase dimple that imprints a λ/4 phase shift in reflection centered on the occulting mask. In the subsequently re-imaged pupil plane, phase errors become intensity modulations. The phase dimple is centered on the focal plane mask, eliminating non-common path errors between coronagraph and wavefront sensor. We measure the wavefront exactly where it matters most. Perhaps even more compelling is that the Zernike sensor is the most sensitive of methods. This is because it is a common-mode interferometer working near the mid-fringe of the interference pattern. Thus, a small phase error is encoded as a small change in pupil intensity in a very efficient way. As indicated earlier, the Zernike sensor has been demonstrated to measure phase with sub-picometer precision [16,17]. Its performance has been demonstrated over a broad spectral band as well.

Expected coronagraph performance. Experiments will be performed in our Compact Coronagraph Testbed (CCT), a laboratory facility to be dedicated exclusively to this task. We expect performance comparable to our recent experiences with the hybrid Lyot coronagraph on the DST [20], which are summarized here.

These recent DST results may be modeled in terms of a contrast floor with the addition of incoherent ghost reflections and scattered light. The coherent component in the coronagraph images can be modeled in terms of a DST testbed and coronagraph elements with known imperfections. The incoherent ghost features and scattered light are not susceptible to modeling due to lack of a sufficiently detailed knowledge of the DST optical path. Instead, we investigate the characteristics of the coherent and incoherent components in the images, seeking further insight into their origins. For this, we make the common assumption that coherent and incoherent signals are equivalent respectively to the components that respond as expected to EFC probing

(the modulated signal) and the components that are unaffected by EFC probing (the unmodulated signal).

Figure 7 illustrates the coherent and incoherent image components in each of the five 2% bands as well as the average of the 2% images comprising the measured contrast across the full 10% band centered on λ_0 = 575 nm, over a 180° dark field extending from 3 to 9 λ_0/D. An analysis of the 2% images was performed, in which the image pixels were binned in circular patches of diameter 1.5 λ_0/D on a sample grid spaced by 0.5 λ_0/D in the x and y directions. The binning is intended to filter the image for intensity features on the approximate scale of a speckle in the coronagraph image. Nevertheless, the results shown here are not sensitive to the precise choices of diameter and pitch of the sample patches. Median intensities are listed for each distribution, and as a check for consistency, the overall NI averaged over the 10% dark field is listed for comparison with the standard FALCO contrast score, which is generally quoted in the literature for DST results.

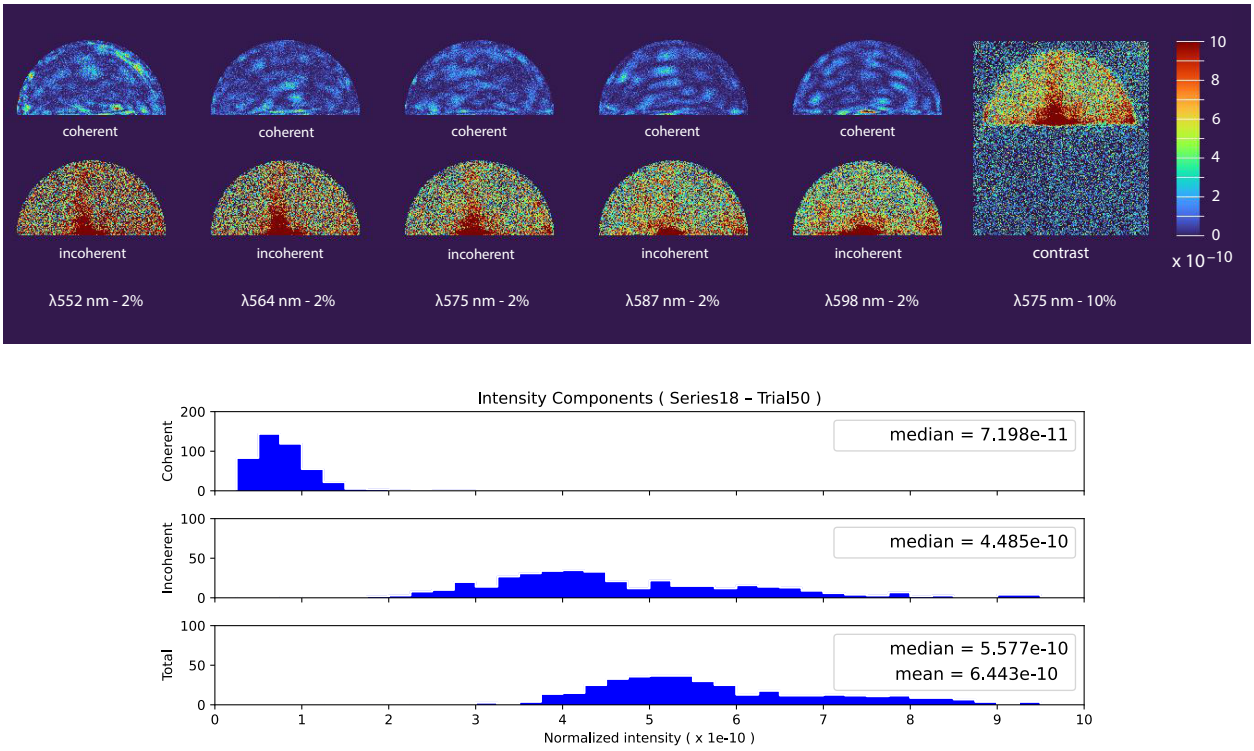

Figure 7. *Representative result from SAT2016 experiments (Series 18-Trial50, August 2023) with the terraced-thickness hybrid Lyot focal plane mask on the DST.*

A set of three histograms accompanies the data set in Figure 7. Histograms of the dark field contrast averaged over these patches are plotted separately for the coherent and incoherent components in the 2% bandpass centered on λ_0, and for the total intensity averaged over the full 10% bandpass. A clear picture emerges in which the (coherent) contrast floor falls within the ~1x10^{-10} range. We interpret this component as indicative of the underlying true contrast floor, i.e., the contrast performance that would be achieved in the absence of scattered background light in the DST. Meanwhile, the ghost and scattered light (incoherent) features appear with

intensities and patterns that vary randomly and capriciously between experiments in the ~4-5x10^{-10} range. This we interpret as originating from poorly understood and non-repeatable internal reflections, scattered light, and other uncertainties in the DST. It is critical to identify and mitigate these experimental testbed factors, which are among those listed in the ***Appendix*** to be addressed as a top priority during the setup of the compact coronagraph in ***Phase 1a***.

The Compact Coronagraph Testbed (CCT) is a laboratory coronagraph with the addition of a steerable mount for the DM, a feature suggested in the ACCESS and Exo-C mission concepts [18,19] to simplify the optical system and reduce the number of optical components in the highly-corrected beam upstream of the coronagraph. Components of the CCT are mounted on a small (34x34x2 inch) vacuum compatible optical breadboard from TMC, which provides flexibility for the component layout and is small enough to be easily transferred as a unit from the in-air clean tent for assembly and alignments, to the vacuum chamber for high contrast demonstrations. The optical path proceeds end-to-end as follows.

Broad band "starlight" originates in a Fianium white light laser, followed by a vis/NIR splitter to separate visible wavelengths from the unwanted NIR radiation. The visible component of the light passes through a Materion interference filter with bandwidth of 11% (or 16%) centered at a wavelength of 550 nm. Out-of-band blocking for the Materion filter is OD8, as required to suppress out-of-band light in the high-contrast dark field. Light then passes through a set of selectable 2% bandwidth filters spanning the Materion bandwidth, as required for EFC and contrast estimation. Filtered light is coupled to a single-mode fiber and passed to a pinhole assembly serving as the surrogate "star." The pinhole assembly reimages the output from the fiber into a 4 μm diameter pinhole, formed on a 1 μm thick layer of silicon nitride (by JPL's Microdevices Laboratory) to minimize waveguide effects, and overcoated with 200 nm of aluminum for opacity. Fiber/pinhole assembly is mounted on a gimbal to allow accurate centering of the output beam on the coronagraph pupil.

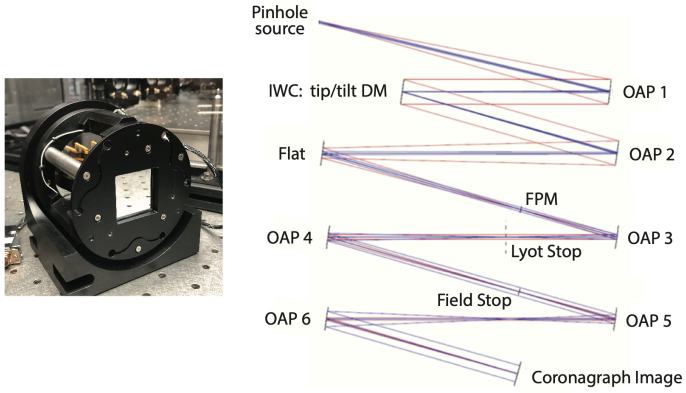

Figure 8. *Optical layout of the compact coronagraph. An integrated wavefront corrector (IWC) is pictured, comprising a high-order deformable mirror mounted in a steerable tip/tilt flexure.*

As shown in Figure 8, CCT is presently configured with six off-axis paraboloidal (OAP) mirrors. Each was manufactured by Space Optics Research Labs (SORL) and cut from a conventionally polished parent paraboloid, a process that minimizes mid-spatial frequency surface figure errors that scatter light into the high contrast dark field. A single 32x32 DM is

mounted as an integrated wavefront corrector (IWC) on a tip/tilt flexure stage manufactured by AOX. The DM is driven by a "Gen5" electronics system developed at JPL with 16-bit DACs and individual amplifiers for each actuator. Located at a pupil, this device becomes the defining pupil of the optical system. Tip/tilt motions are used to center the "star" image on the focal plane mask (FPM), or to simulate line-of-sight offsets. The Lyot stop is a thin blackened sheet with a circular aperture. Field stop is cut into a thin blackened sheet to reduce stray light near the dark field. The high contrast dark field is imaged on a 1Kx1K back-illuminated CCD from e2V, which is TEC cooled and encapsulated with its low-noise front-end electronics for operation in air or vacuum.

For the proposed demonstrations, the CCT will be reconfigured with an additional pair of OAPs as indicated in the Figure 1 sketch, providing an additional pupil where the LOWFC assembly is located. With a single 32x32 high-order DM, we use the system to create a 180° dark field, which is the simplest mode for the demonstration. A second 32x32 DM could be added, enabling a full 360° dark field, but this added complexity is not required to test the LOWFC concept.

Exoplanet Imaging Technology Laboratory. The CCT coronagraph components will be characterized, assembled, and tested with the facilities resident in the Exoplanet Imaging Technology Laboratory. This facility has been developed by the PI specifically to advance enabling technologies for high contrast imaging from a space observatory, most notably fabrication and testing of HLC focal plane masks and the characterizations of deformable mirrors to picometer levels in a stable vacuum environment. As in the past, this laboratory will be used to exercise a new technology, identify problems and devise solutions, carry out characterizations at the required levels of wavefront control and high contrast imaging and make detailed comparisons with model expectations, ultimately to validate the concept and advance its TRL. At the completion of this task, we will evaluate the LOWFC element in terms of its relevance to the next generation of space coronagraph observatories, and specifically to the requirements of the HWO flagship mission. We will also consider promoting the LOWFC technology for use in the ExEP Decadal Survey Testbeds, enabling use by the wider community and potentially higher levels of experimentally validated performance.

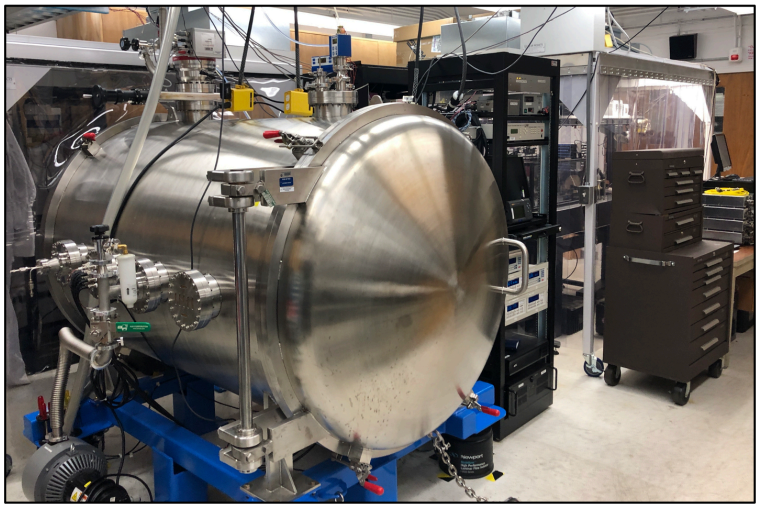

Figure 9. *Exoplanet Imaging Technology Laboratory. Left to right: 4x6 foot vacuum chamber, electronics racks, and the clean-tented 4x6 foot optical table.*

5) Data Measurement & Analysis

Contrast is defined as the average intensity of the residual light (speckles, diffracted starlight, etc.) within the dark field, relative to the peak intensity of an image of the source/star. Multiple successive measurements, each obtained following a sequence of EFC iterations, and repeated from scratch (DMs set to flat) at least three times, are taken to establish reliability. The distribution of contrast measurements is regarded as Gaussian about a mean contrast for the data set, which represents the true contrast value. A Student's t-distribution is used to estimate confidence coefficients on the assumption of Gaussian statistics.

Measurement of the Star Brightness. The "star" is a small pinhole illuminated with light relayed via single-mode optical fiber from a source outside the vacuum wall (e.g., a filtered super-continuum white light source). This star is the only source of light in the optical path of the testbed. Star brightness is the peak intensity of the star image measured in the fully assembled coronagraph with just the FPM removed (e.g., laterally offset by ~6 λ/D) and no longer occulting the star. A photometry ladder is established to account for the dynamic range of the detector and linear range of exposure times available with the shutter. For example, the FPM can be offset from the star in steps, revealing the full intensity in steps, each of which can be measured in long and short exposures within the dynamic range of the detector and exposure times within the linear range of the shutter.

Measurement of the Coronagraph Dark Field Contrast. With the FPM centered on the star, images are acquired of the coronagraph field, which includes the suppressed star, dark field, and the surrounding speckle field outside the Nyquist radius. In previous SAT experiments, we have found the surrounding speckle field (red area in Figure 10) to be unchanged by the insertion or removal (by lateral translation) of the FPM or by nominal adjustments in the DM surface figure, hence each image captures an intensity metric with a known and fixed ratio to the star intensity. The contrast field is a map of detector pixel values (bias subtracted and flat-field normalized) divided by the peak star value estimated as a ratio to the average intensity measured over the surrounding speckle field.

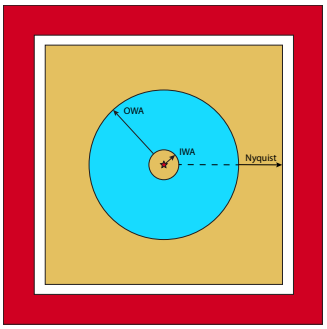

Figure 10. *Definition of the target high-contrast dark field. The occulted star is at the center of the diagram. A 360° high contrast dark field (in blue) extends from the inner working angle (IWA) to the outer working angle (OWA). The speckle control region (in yellow) is square and extends to the Nyquist limit (angular distance from the star to the nearest side = Nλ/2D, where N is the actuator count across the DM). The reference field for contrast photometry (in red) is an area of uncontrolled speckles beyond the Nyquist boundaries.*

Demonstration of low-order wavefront control. The objective is to introduce, sense, and correct low-order wavefront errors with minimum disruption of the high contrast dark field. A static contrast of $5x10^{-10}$ is called for, extending from 3 to 10 λ_0/D, in a 10% spectral band centered at 550 nm, and stable to $\pm 1x10^{-10}$ or better, assuring that the effects of SPA/DM activity on contrast can be measured at a significant level. The sequence of laboratory tasks and experiments leading to the milestone demonstrations is as follows.

Phase 1a -- Assemble and align the CCT. Objective is to finalize optical design and testbed layout, acquire necessary components, mount and align the coronagraph elements, and verify functionality in the ambient laboratory environment.

Phase 1a,b -- VSG calibrations of the SPA/DM and the high-order DM. Objective is the characterization of the deformable mirrors to be used in these demonstrations, taking advantage of the Vacuum Surface Gauge (VSG) facility resident in the PI's laboratory. Calibration of the high order 32x32 DM can begin immediately (Phase 1a), with emphasis on actuator voltage settings for flat and low order patterns on the high-order DMs. Calibrations of the SPA/DM can commence once the SPA/DM has been received (Phase 1b). A sequence of standard tests will be performed as follows.

- Surface maps at zero volts
- Surface shape (influence profile) for all actuators
- Actuator displacement vs. voltage curves
- Flat surface solution at specified bias voltage
- Actuator drift/settling coefficients and repeatability of the flat surface solution
- Low order Zernike surface shapes (~1 nm rms Z4-Z8 (focus, astigmatism, and coma).
- Flat surface setting in ambient (air) environment

Phase 2a --Tip/tilt pointing control. Objective is to calibrate and demonstrate the tip/tilt control feature of the LOWFS&C system. This can be performed in the ambient laboratory environment during setup and alignment of the CCT.

- Command tip/tilt offset of the 'star' with the SPA flexure mount (sequester the command)
- Use ZWFS to sense the tip/tilt offset
- Correct the offset via ZWFS-derived command to the flexure mount

Phase 2a --Closed loop ZWFS – SPA/DM performance in vacuum. Objective is to establish internal consistency between sensing and control in the ZWFS – SPA/DM control loop. Preliminary tests can be performed in the ambient laboratory, but ultimately performance is confirmed in the vacuum environment.

- Start with a nominal flat voltage setting on the SPA/DM
- Use pairwise probing/EFC to establish a high contrast dark field
- Sense the low order wavefront with the ZWFS to establish the ZWFS reference baseline
- ***Command a low order Zernike error on the SPA/DM (and sequester the command).***
- Use ZWFS to sense the low order wavefront error and correct the error with the SPA/DM.
- Measure dark field contrast, quantify differences from the original dark field
- Use pairwise probing/EFC to re-establish (clean up residual errors in) the dark field.

- Analyze the high-order DM voltage settings required for the EFC clean-up, use high-order DM calibration data to infer the residual wavefront error.

Phase 2b -- Low order sensing and correction in vacuum. ***Objective is to use ZWFS and SPA/DM to sense and correct a clean low order Zernike error introduced independently by the high-order DM***. This experiment exploits the independence of the legacy pairwise-probing/EFC and the new ZWFS&C wavefront sensing and control methods.

- Start with a nominal flat setting on the SPA/DM
- Use pairwise probing/EFC to establish a high contrast dark field
- Sense the low order wavefront with the ZWFS to establish the ZWFS reference baseline
- ***Command a low-order Zernike error with the high-order DM. (Success requires excellent calibration of the high-order DM.)***
- Use ZWFS to sense the changes in wavefront and correct the error with the SPA/DM
- Measure dark field contrast, quantify differences from the original dark field
- Use pairwise probing/EFC to clean up any residual wavefront errors and re-establish the original dark field.
- Analyze the high-order DM voltage settings required for the EFC clean-up, use high-order DM calibration data to infer the residual wavefront error.
- These demonstrations to be repeated three times.

6) Success Criteria

The milestones defined in Section 3 cover the preparation, calibrations, and testing of hardware and software as required for the demonstration of active low-order wavefront control in a high-contrast coronagraph. The wavefront control system is exercised in an final end-to-end demonstration of high-contrast coronagraph imaging and control of low-order wavefront errors.

Phase 1a Milestone. Upgrade the CCT and verify end-to-end functionality. This milestone marks completion of the design and procurement of coronagraph and wavefront control elements required for the final demonstrations. The reconfigured CCT demonstrates baseline static contrast performance of $5\text{x}10^{-10}$ extending from 3 to 10 λ_0/D, in a 10% spectral band centered at 550 nm.

Phase 1b Milestone. Verify CCT baseline performance; test and calibrate the SPA/DM. Milestone marks the procurement and calibrations of the new low-order deformable mirror element -- a new technology fundamental to the final demonstrations. SPA/DM has been specified, manufactured, and received from AOX. Calibration of the SPA/DM has been performed in the dedicated vacuum interferometer.

Phase 2a Milestone. Demonstrate closed-loop wavefront control with SPA/DM. Demonstrates the functionality of the ZWFS control loop, verifies that the testbed hardware and all software elements are in place and ready for the final demonstrations. The Zernike wavefront sensor has demonstrated sensitivity consistent with the accuracy of the 16-bit SPA/DM driver electronics.

Phase 2b Milestone. Low-order wavefront stabilization concurrent with high-contrast imaging. The demonstration of a new ZWFS&C element that effectively separates static high-

order and active low-order wavefront control elements in a high-contrast coronagraph testbed which is sensitive and diagnostic to wavefront errors at levels relevant for exoplanet imaging.

The CCT+SPA/DM system has demonstrated wavefront control and high-contrast coronagraph performance in the presence of low order disturbances of 1 nm rms or more, with sufficient fidelity to maintain coronagraph contrast of $5x10^{-10}$ or better over a dark field extending from 3 to 10 λ/D, in a 10% spectral band centered at 550 nm.

7) Schedule

The sequence of tasks leading to the milestone demonstrations is shown in the schedule. Scheduled activities can begin once the first-year funding is received.

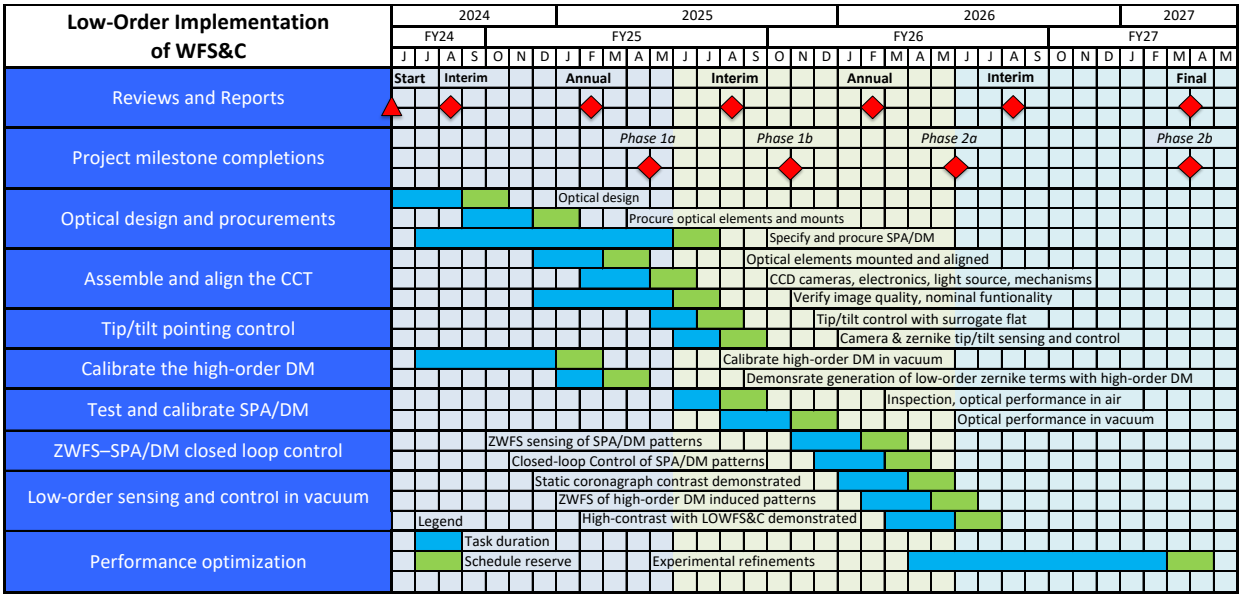

8) References

1. National Academies of Sciences, Engineering, and Medicine, 2021. *Pathways to Discovery in Astronomy and Astrophysics for the 2020s.* Washington, DC: The National Academies Press. https://doi.org/10.17226/26141.
2. N.J. Kasdin et al. 2020. "The Nancy Grace Roman Space Telescope Coronagraph Instrument (CGI) Technology Demonstration." SPIE, https://doi.org/10.1117/12.2562997.
3. B. Crill, 2022. "Progress in Technology for Exoplanet Missions, an Appendix to the NASA Exoplanet Exploration Program Technology Plan." JPL Document D-108825, https://exoplanets.nasa.gov/exep/resources/documents/.
4. Mawet et al., 2012. "Review of small-angle coronagraphic techniques in the wake of ground-based second-generation adaptive optics systems." SPIE, https://doi.org/10.1117/12.927245.
5. J.W. Goodman, 1988. "Introduction to Fourier Optics, Second Edition." McGraw Hill Companies, New York.
6. L. Pueyo, J. Kay, N.J. Kasdin, T. Groff, M. McElwain, A. Give'on, and R. Belikov, 2009. "Optimal dark hole generation via two deformable mirrors with stroke minimization," Applied Optics 48, https://doi.org/10.1364/AO48.006296.
7. J. Krist, B. Nemati, and B. Mennesson, 2015. "Numerical modeling of the proposed WFIRST-AFTA coronagraphs and their predicted performances." JATIS, https://doi.org/10.1117/1.JATIS.2.1.011003.
8. T.D. Groff, A.J. Riggs, B. Kern, and N.J. Kasdin, 2015. "Methods and limitations of focal plane sensing, estimation, and control in high-contrast imaging," JATIS 2, https://doi.org/10.1117/1.JATIS.2.1.011009.
9. WFIRST Coronagraph Testbed and Modeling Teams, 2017. "WFIRST CGI Milestone 9, Dynamic Contrast Demonstration Status Update." https://exoplanets.nasa.gov/exep/resources/documents/Coronagraph Milestone 9.
10. J. Trauger et al., 2011. "A hybrid Lyot coronagraph for the direct imaging and spectroscopy of exoplanet systems: recent results and prospects." SPIE, https://doi.org/10.1117/12.895032; and J. Trauger et al., 2012. "Final Report: Advanced Hybrid Lyot Coronagraph for Exoplanet Missions." https://exoplanets.nasa.gov/exep/technology/TDEM-awards.
11. B-J. Seo et al., 2019. "Testbed demonstration of high-contrast coronagraph imaging in search for Earth-like exoplanets." SPIE, https://doi.org/10.1117/12.2530033.
12. The LUVOIR Team, 2019. "The LUVOIR Mission Concept Study Final Report." https://doi.org/10.48550/arXiv.1912.06219.
13. B. Scott Gaudi et al., 2020. "The Habitable Exoplanet Observatory (HabEx) Mission Concept Study Final Report." https://doi.org/10.48550/arXiv.2002.06683.
14. A. Wirth, J. Cavaco, T. Bruno, and K. Ezzo 2013. "Deformable Mirror Technologies at AOA Xinetics." SPIE, https://doi.org/10.1117/12.2018031.

15. M. N'Diaye, K. Dohlen, T. Fusco, and B. Paul, 2013. "Calibration of quasi-static aberrations in exoplanet direct-imaging instrument with a Zernike phase-mask sensor." Astronomy and Astrophysics 555, https://doi.org/10.1051/0004-6361/201219797.
16. G. Ruane, J.K. Wallace, J. Steeves, et al., 2020. "Wavefront sensing and control in space-based coronagraph instruments using Zernike's phase-contrast method." JATIS, https://doi.org/10.1117/1.JATIS.6.4.045005.
17. J. Steeves, J.K. Wallace, C. Kettenbeil, and J. Jewell, 2020. "Picometer wavefront sensing using the phase-contrast technique." Optica 7, https://doi.org/10.1364/OPTICA.398768.
18. K.R. Stapelfeldt et al., 2014. "Exo-C: a probe-scale space mission to directly image and spectroscopically characterize exoplanetary systems using an internal coronagraph." SPIE, https://doi.org/10.1117/12.2057115.
19. J. Trauger et al., 2009. "ACCESS – A concept study for the direct imaging and spectroscopy of exoplanetary systems," SPIE, https://doi.org/10.1117/12.858301.
20. J. Trauger et al., 2018. "Super Lyot ExoEarth Coronagraph." https://exoplanets.nasa.gov/exep/technology/TDEM-awards/ TDEM_Trauger_WP.pdf.
21. A.J. Eldorado Riggs et al., 2018. "Fast linearized coronagraph optimizer (FALCO) I: a software toolbox for rapid coronagraphic design and wavefront correction." SPIE, https://doi.org/10.1117/12.2313812.
22. D.C. Moody et al., 2018. "Fast linearized coronagraph optimizer (FALCO) II: optical model validation and time savings over other methods." SPIE, https://doi.org/10.1117/12.2312950.
23. C.T. Coker et al., 2018. "Fast linearized coronagraph optimizer (FALCO) III: optimization of key coronagraph design parameters." SPIE, https://doi.org/10.1117/12.2313788.
24. A.J. Eldorado Riggs et al., 2018. "Fast linearized coronagraph optimizer (FALCO) IV: coronagraph design survey for obstructed and segmented apertures." SPIE, https://doi.org/10.1117/12.2312973.
25. K. Balasubramanian et al., 2019. "Critical characteristics of coronagraph masks influencing high-contrast performance." SPIE, https://doi.org/10.1117/12.2530825.
26. E. Sidick et al. 2017. "Optimizing the regularization in the broadband wavefront control algorithm for the WFIRST coronagraph." SPIE, https://doi.org/10.1117/12.2274440.

9) Acknowledgements

Many thanks to Brendan Crill and members of the ExoTAC review board for valuable comments and recommendations. This research was carried out at the Jet Propulsion Laboratory, California Institute of Technology, under a contract with the National Aeronautics and Space Administration (80NM0018D0004).

10) Appendix: Testbed Performance Factors

A number of experimental factors critical to coronagraph testbed performance are collected here, to be addressed in the setup of the compact coronagraph testbed (CCT). Each of these factors has the potential to degrade demonstrated contrast at ~10^{-10} levels. Some have been observed and quantified in previous work, such as the DST commissioning experiments. Some can be estimated from model predictions, and a significant number of them are not well-quantified, even for the DST. These factors are related to the quality of the optical elements, alignments, ghost images and stray light, and are applicable to any coronagraph configuration, whether Lyot, vortex, or other types. These factors tend to add incoherently to the total background intensity in the high-contrast dark field. Steps to be taken to mitigate these limiting factors are mentioned item-by-item in the following paragraphs.

1. ***Ghost reflections*** from the backside of the FPM substrate. Commissioning DST demonstration with a classic Lyot FPM was estimated to contribute 1.0×10^{-10} to the dark field contrast [11]. Remedies include: a 0.8° wedge in the substrate to separate the backside beam from the main central beam, baffle at OAP3 to remove ghost beam from the optical system, and low-reflectance AR coating on the backside of the FPM.

2. ***Multiple internal reflections*** need to be minimized among the shiny coronagraph elements that are nearly normal to the beam in the coronagraph optical system, as illustrated for the case of DST in ***Figure A1*** below. These elements are the source pinhole, the FPM substrate, Lyot stop, field stop, and the CCD focal plane. Remedies include blackening and optimal off-axis tilts for these elements and the addition of baffles as appropriate.

3. ***Scatter by particulate contamination*** on elements near focal planes, including the FPM and elements in the imaging sensor. Remedies include a cleanliness protocol supported by close in-situ inspection of the elements under bright light and magnification.

4. ***Line-of-sight jitter***, which was estimated to contribute dark field background at the 0.4×10^{-10} contrast level in the DST commissioning demonstration [11]. Remedies include vibration isolation (e.g., the CCT vacuum chamber is on vibration damping air legs, the coronagraph optical table is on elastomeric dampers) and isolation of sources of vibration on the optical table (such as the shutter), as verified with accelerometers in the chamber.

5. ***Chromaticity of the coronagraph elements*** over the 10% bandwidth, which was estimated to contribute 0.9×10^{-10} to the dark-field background with the classic Lyot FPM in the DST commissioning experiment [11]. Mitigation must be a part of coronagraph design, including consideration of dispersion in the refractive index of FPM optical materials and DM surface patterns for high contrast.

6. ***Least Significant Bit in the DAC*** and electrical noise in the DM driver, which was estimated to contribute 0.9×10^{-10} to the contrast in DST commissioning [11]. Mitigations include working at a minimal DM bias voltage (reduced gain/volt due to quadratic response of AOX DMs), reduced maximum power supply voltage to reduce the magnitude of the LSB voltage step, and adoption of a driver with more digital resolution (i.e., 20 bits rather than standard 16 bits).

7. ***Polarization and birefringence due to FPM substrate*** index inhomogeneity, which was estimated to contribute 1.2×10^{-10} to the contrast during DST commissioning [11,25]. Mitigations

include choice of highest-homogeneity/lowest birefringence substrate material (e.g., Corning class 0A fused silica) and minimum substrate thickness.

8. ***Other polarization effects*** include the cumulative polarization state created by bare-aluminum-coated OAP and tilted mirror elements, as well as inadvertent vignetting and glints from hardware in or near the optical beam, as evidenced in the DST by the reduction in incoherent background (typically by a few $x10^{-10}$) when an analyzing polarizer is inserted near the tail end of the optical path. Polarization effects for bare aluminum mirror coatings are predictable and polarization performance of the coronagraph can be quantified by ray-trace analysis.

9. ***Source pinhole irregularities***, waveguide effects, nonuniformity of pupil illumination, which was estimated to contribute up to $1x10^{-10}$ in DST commissioning demonstrations [11]. Mitigations include custom pinhole fabrication at JPL's Micro Devices Laboratory, selected for best quality, such as a 4-micron diameter pinhole, waveguide effects minimized with pinhole cut into a 1-micron-thin silicon nitride material, opaque surrounding surface (200 nm thickness aluminum coated layer for opacity), illumination from single mode fiber coupler well-centered on the pinhole, uniform illumination of the entrance pupil illumination via steerable pinhole source assembly. Pinhole is a source of polarization cross terms.

10. ***Optimal FALCO EFC parameters and β-bump schedule.*** Experimentation with the β-bump schedule is recommended for best achieved contrast [26].

11. ***Focal Plane Mask manufacturing imperfections***. Keep imperfections within model tolerances, include measurement of critical characteristics as feedback for manufacturing refinements. The hybrid Lyot FPM is minimally complex, and optical simplicity minimizes avenues for potential imperfections.

12. ***Red leak background*** in the spectrum of source illumination is a critical concern at inner working angles in the dark field. Model calculations (D. Moody, internal communication, 2014) lead to requirements for off-band rejection of 10^{-8} or better and a sharp red cutoff in the bandwidth-defining spectral filters. The red-leak requirements can be met with well-blocked commercial bandpass filters, such as obtained in the past from Materion.

13. ***Imaging sensor scattered light and pixel crosstalk.*** A CMOS camera, for example, introduces scatter from lenslets, focal plane micro-structure, and reflections from a vacuum window which have not been accurately modeled. A back illuminated CCD may be preferable for minimal scatter and crosstalk. This experiment utilizes a TEC-cooled, back-illuminated 1Kx1K e2V CCD packaged together with its low-noise electronics in a vacuum compatible enclosure.

14. ***Minimum number of transmissive optics*** in the highly corrected beam upstream of the focal plane mask. Transmissive elements introduce dispersion in refractive index, birefringence, scatter, and ghost reflections. The hybrid Lyot coronagraph has only one transmissive element, the FPM, which can be AR coated and made of highest homogeneity fused silica.

15. ***DM inter-actuator creep*** is a well-known characteristic of the PMN electroceramic actuators, as observed with AOX DMs and Gen5 electronics drivers. Mitigations include ring-in sequences when changing voltage settings, minimization of large voltage swings, maintenance of continuous power to the DM, thermal control on mounts and electronic interconnect cables, and

a temperature-controlled DM enclosure to restrict the DM's thermal coupling to the ambient surroundings.

16. ***Low-order aberrations due to alignment drift*** calls for stable mounting hardware, temperature regulation in the testbed laboratory, and closed loop temperature control of the critical active optics (DM, tilt stage).

17. ***Ambient air turbulence.*** Operate in vacuum chamber (e.g., Exoplanet Imaging Technology Laboratory turbo-pumped vacuum chamber operates at ~5x10^{-7} torr).

Figure A1. Ghost Reflections. Our previous DST experience [20] suggests that ghost images due to near-normal internal reflections within the coronagraph will create incoherent scattered background and compromise the achieved testbed contrast. This can be mitigated in our CCT experiments by a combination of blackening and tilting of these five elements, together with a baffle at OAP3 and other locations as required.

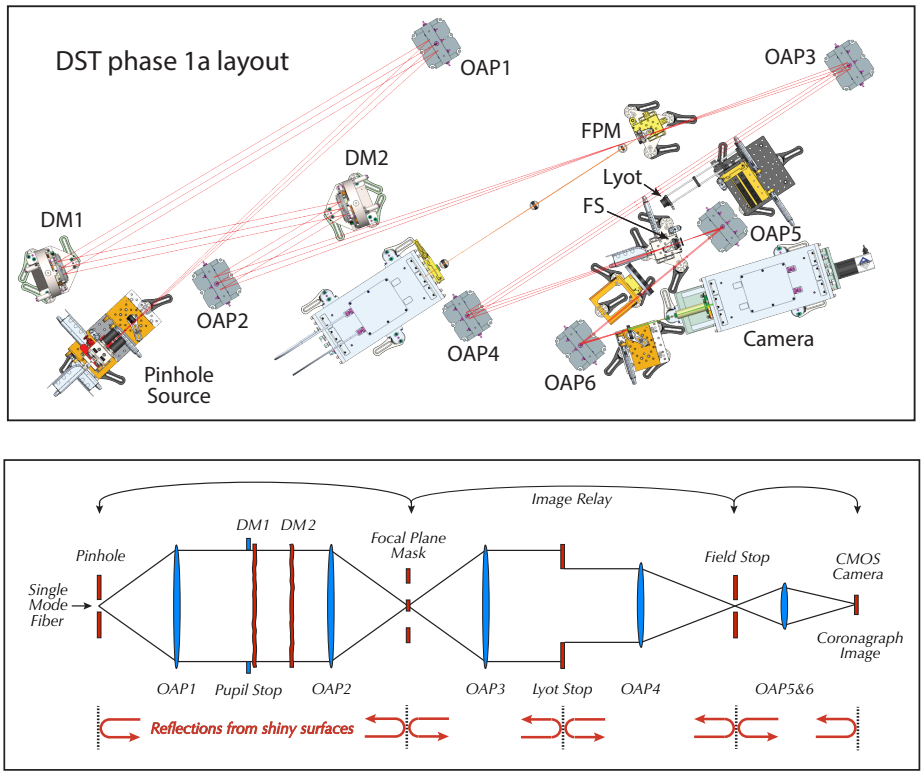

Figure A1. *Potential for ghost images created by near-normal internal reflections in the coronagraph optical path, as experienced in earlier DST experiments. The upper graphic identifies the elements of the DST coronagraph. Below is a sketch of the optical path unfolded for clarity. The five critical reflective surfaces are indicated by the vertical dashed lines at the bottom of the sketch, with arrows indicating internal reflections that are guaranteed to happen at these surfaces.*

As indicated in Figure A1, each of five reflective elements can relay a focused speckle-sized feature from one focal plane to another. For example, light reflecting from the Lyot stop can return to the FPM, where the in-focus feature can reflect from the FPM and add an incoherent feature to the coronagraph image. Or a fraction of the light at the focal plane of the CMOS camera can reflect back to the field stop, then return in-focus to the CMOS focal plane. Etc. Such effects are not negligible for light suppression at the 10^{-10} levels.

This will be addressed in the initial setup of the CCT in terms of blackening and tilting of the elements to minimize the internal reflections.

11) Acronyms

ACCESS	Actively Corrected Coronagraph for Exoplanet System Studies
AOX	Adaptive Optics Associates - Xinetics (Northop Grumman)
CCT	Compact Coronagraph Testbed
CCD	Charge Coupled Device
CGI	Coronagraph Instrument on the Nancy Grace Roman Observatory
CMOS	Complementary Metal Oxide Semiconductor
DAC	Digital to Analog Converter
DM	Deformable Mirror
DST	Decadal Survey Testbed managed by the Exoplanet Exploration Program
EFC	Electric Field Conjugation
ExEP	Exoplanet Exploration Program
ExoTAC	ExEP Technology Assessment Committee
FALCO	Fast Linearized Coronagraph Optimizer
FCM	Focus Control Mechanism
FPM	Focal Plane Mask
FSM	Fine/Fast Steering Mirror
HLC	Hybrid Lyot Coronagraph
HWO	Habitable Worlds Observatory
IWA	Inner Working Angle
IWC	Integrated Wavefront Corrector
LOWFC	Low Order Wavefront Control element
LOWFS	Low Order Wavefront Sensing
MLI	Multilayer insulation
OAP	Off Axis Paraboloidal mirror
PSF	Point Spread Function
PMN `	Lead Magnesium Niobate electrostrictive ceramic
SPA/DM	Surface Parallel Actuated Deformable Mirror
TEC	Thermal Electric Cooler
TMC	Manufacturer of optical breadboard tables
VSG	Vacuum Surface Gauge
ZWFS	Zernike Wavefront Sensor
ZWFS&C	ZWFS + LOWFC sensing and control system